NIPPON STEEL TECHNICAL REPORT No. 83 JANUARY 2001

UDC 669 . 782 : 620 . 19

Micro-fluctuation of Growth Rate and Grow-in Defect Distribution in CZ-Si

Jun FUKUDA*1
Toshio IWASAKI*1
Masahiro TANAKA*2
Koichi KITAHARA*2
Masami HASEBE*1
Hirofumi HARADA*1
Katsuhiko NAKAI*2

Abstract

Using a device to apply a horizontal magnetic field, the authors created CZ crystals having peculiar "galactic" or "double helix" distribution patterns of grown-in defects in the silicon wafers. The grown-in defect formation and distribution mechanisms have been examined using a parameter called V/G proposed by Voronkov and widely applied to the control of microscopic distribution of the defects. The authors evaluated the crystals having the peculiar defect distributions in detail to study the defect formation mechanisms not accounted for by the parameter V/G. This paper proposes formation of the generation sites of uneven defect nuclei utilizing microscopic fluctuations of temperature and growth rate at the crystal solidification boundary. Control of the nuclei generation sites besides the Voronkov's parameter may lead to a new defect control technique.

1. Introduction

Since 1990, point defects and grown-in defects of silicon crystals have been listed among principal subjects of many researchers in view of achieving high gate oxide integrity (GOI) of the crystals for 4 MB DRAMs and higher integration devices[1-5]. Studies of the grown-in defect identification started with the discovery of crystal originated pits (COPs) by Ryuta et al.[6], then, for clarifying the mechanisms of defect formation and distribution, numerous investigations were made on CZ crystals grown under various conditions such as rapid cooling of crystals by forced detachment from the melt, changes of growth rates, holding of growth, etc. Studies were also made regarding oxidation-inducted stacking faults (OSFs) formed inside silicon wafers in a ring shape (R-OSFs) and the GOI properties of CZ wafers[7-9].

In view of test results, models on point defect interactions and defect distribution during crystal cooling were proposed by Petroff et al.[10], Voronkov[11], and Habu et al.[12] for the purpose of clarifying mechanisms of the macroscopic defect distribution. Although there are some disagreements among these models about the introduction and movements of point defects during crystal growth, the so-called Vononkov's parameter V/G (where V is crystal growth rate and G is crystal temperature gradient near solidification boundary) is generally accepted as a factor to determine macroscopic defect distribution. It has been made clear that the inside of crystals can be classified, according to the value of V/G, into a vacancy-rich region (COP region), a neutral region (region where vacancies and interstitial atoms are well balanced), and an interstitial atom-rich region (interstitial loop region).

In the meantime, microscopic distribution of the grown-in defects has been discussed in relation with concentric striation patterns caused by microscopic fluctuation of crystal growth rate. FZ crystals contain defects called A swirl and B swirl identified as interstitial atom-induced defects[13]. Chikawa et al. proposed a nucleation model of these defects in 1970[14], maintaining that melt droplets formed in

*1 NSC ELECTRON CORPORATION, Presently Wacker NSCE Corp.
*2 Technical Development Bureau

crystals by partial remelting during crystal growth worked as nuclei of the A and B swirl defects. As for the vacancy type defects know as D defects often seen with fast grown FZ crystals, it has been made clear that they did not take a swirl distribution pattern[15], although microscopic distribution mechanisms of these defects have not been clarified.

With regards to the CZ crystals, concentric swirl distribution of oxygen precipitates was confirmed and their nucleation models (homogeneous and heterogeneous nucleation models) were discussed in the 1970s and 1980s[16-19]. It was in the early 1990s that vacancy type grown-in defects were found to exist for the first time in the CZ crystals after the COP defects were discovered[20]. COPs are a vacancy type void defect of an octahedral shape bounded by eight (111) planes of silicon crystal. It has been made clear that many COPs are seen to have their vertices cut by (100) planes and the interior surface of the defects is covered with an oxide film several nanometers in thickness[21,22].

A striation distribution of COPs, a vacancy type defect, in CZ crystals was reported in 1991 by Yamagishi et al.[23], in 1993 by Umeno et al.[24], and in 1994 by Nakajima et al[25]. Since then their distribution has been discussed in relation with distribution fluctuation of dopant or oxygen during crystal growth and changes in crystal cooling rate[26-30]. However, no definitive conclusion has been reached yet as to how the defect distribution is formed, especially on the relationship between macroscopic distribution of point defects and microscopic distributions of dopants and oxygen impurities changing according to crystal growth conditions.

We have succeeded in intentionally forming defect distribution patterns through control of melt flow and temperature distribution using horizontal magnetic field-applied Czochralski (HMCZ). This paper describes: (1) calculation of microscopic crystal growth fluctuation from measurements of melt temperature distribution and the shape of crystal solidification boundary; and (2) examination of the relationship between defect distribution and distribution of dopants and oxygen impurities of the crystals having the intentionally introduced defect distributions. Furthermore, based on analysis of the test results and computer simulations on the above subjects, this paper proposes and discusses a model of grown-in defect formation mechanism.

2. COP Distribution in Crystals with Intentionally Introduced Defect Distribution

Fig. 1 shows examples of the intentionally formed COP distribution patterns, wherein (a) is a "milky way" pattern and (b) is a "double spiral" pattern. COPs larger than 0.11 μm were counted using a Hitachi LS6000 particle counter. The wafers used herein were sliced out from the HMCZ crystals grown under application of a horizontal magnetic field 0.3 T in intensity at a crystal rotation of 0.1 rpm.

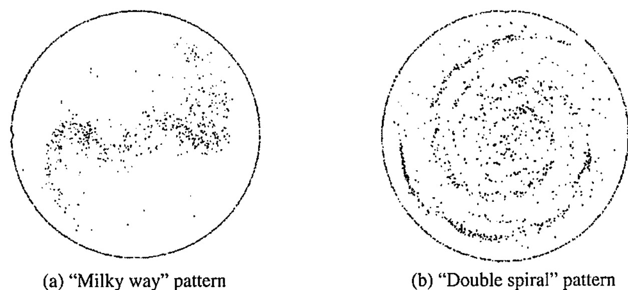

(a) "Milky way" pattern (b) "Double spiral" pattern

Fig. 1 COP distribution

3. CCD Observations of Melt Temperature Distribution

In the first place, temperature distribution at the melt surface during crystal growth was measured with an infrared CCD camera system for the purpose of a 3-D analysis of defect distribution in the silicon crystals. The CCD camera was placed at the top of a pull furnace and a transparent quartz plate was put on the melt surface as an imitation crystal. **Fig. 2** (a) shows an observation result wherein a CCD video image is converted into a melt temperature distribution image. The observation condition was: crucible diameter 22", crucible rotation 4.0 rpm, crystal rotation 0 rpm, and magnetic field intensity 0.3 T. Distribution of low temperature regions of the melt is shaped in a 2-fold symmetry, the low temperature region being stretched along the horizontal magnetic field in a rugby ball shape.

A closer look reveals that the low temperature region is twisted by a fixed angle in the crucible rotation direction, showing that the melt surface is dragged by the crucible rotation. When a crystal is grown at a very slow crystal rotation of 0.1 rpm under this melt condition designed for the test, the crystal solidification boundary feels a low temperature region and a high temperature region in alternation. When the crystal rotation is pulled to about 10 rpm, however, the solidification boundary does not feel the alternate low and high temperature change but an averaged temperature due to a melt agitation effect of the crystal itself.

4. Geometrical Analysis of Defect Distribution

Then, we studied defect distribution of the crystals grown under the above special test condition. First, based on the temperature distribution of the melt measured with the CCD camera, it was supposed that a fixed defect formation band existed along the horizontal magnetic field (Fig. 2 (b)). A double spiral structure shown in Fig. 2 (c) is obtained by geometrically developing the defect band in the crystal growth direction while rotating it. The "milky way" pat-

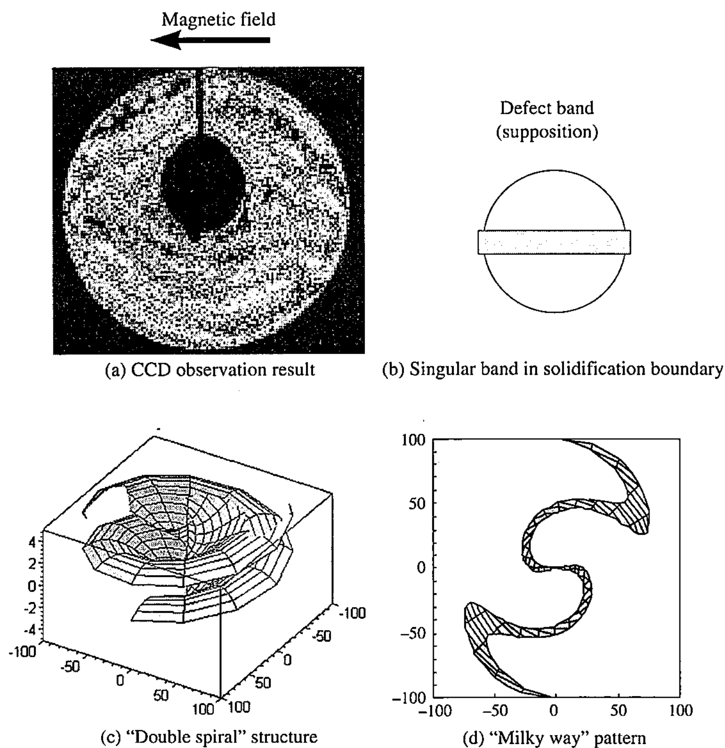

(a) CCD observation result (b) Singular band in solidification boundary

(c) "Double spiral" structure (d) "Milky way" pattern

Fig. 2 CCD observation result and geometrical analysis of COP

tern shown in Fig. 2 (d) is obtained when the double spiral structure is sliced by a plane parallel to the melt surface (vertical to the crystal growth direction). The pattern changes when the shape of the solidification boundary changes: the "milky way" pattern is obtained through a geometric calculation based on an assumption of an M-shaped boundary, whereas the "double spiral" patter is obtained at a sectional plane on an assumption of a concave boundary shape. Thus, unique defect distribution patterns shown in Fig. 1 can be geometrically reproduced by supposing a band correlated with temperature distribution at the crystal growth solidification boundary. Physical influence of the band unique to HMCZ on the crystals is discussed later together with defect distribution evaluation.

5. Estimation of Growth Rate Changes by Measurement of Solidification Boundary Shape

Fig. 3 (a) is a photograph of an outside appearance of a 200-mm diameter crystal grown under the above-mentioned condition, i.e., 22" diameter crucible, crystal rotation 0.1 rpm, crucible rotation 1.0 rpm, magnetic field intensity 0.3 T, and pulling rate 0.65 mm/min. The crystal surface has periodical undulations formed with two spirals not crossing each other (double spiral) as schematically shown in Fig. 3 (b) (this type of crystal being hereinafter called the "spiral crystal"). The gap between the undulations is 6.5 mm, corresponding to the length of crystal growth in 1 rotation. The salient portions of the side surface are grown in the low temperature regions of the 2-fold symmetric distribution of the melt surface, and the recessed portions in the high temperature regions.

The crystal solidification boundary was measured 3-dimensionally for the purpose of examining the change in the crystal growth rate. The crystal solidification boundary was severed from the melt during growing for the measurement. **Fig. 4** (a) shows contours of the solidification boundary surface seen from below. The section is not in a perfect circle but an ellipse. Scanning the fluctuation of boundary height in the circumferential direction, we see that the boundary surface is high in the low temperature region of the melt and it is low in the high temperature region, corresponding to the 2-fold symmetric melt temperature distribution. Fig. 4 (b) shows the measurement result. Fig. 4 (c) is the crystal height fluctuation differentiated by the time calculated from the pulling rate, showing the change in the growth rate. It can be seen here that a growth rate change of minus 0.8 mm/min occurred at the position where the boundary height is small, namely, the growth rate is low. From the fact that its absolute value is larger than the pulling rate 0.65 mm/min, it was understood

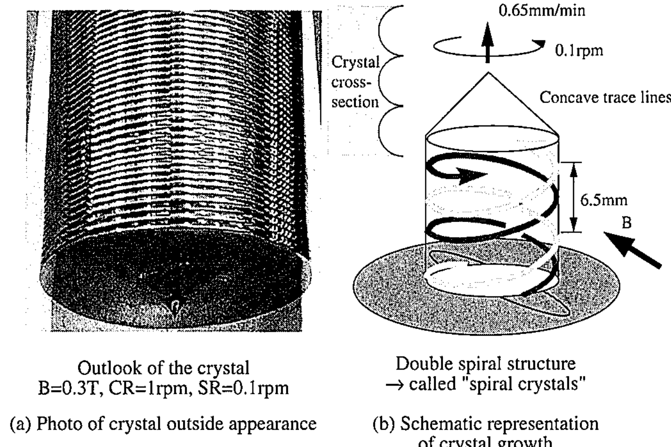

(a) Photo of crystal outside appearance (b) Schematic representation of crystal growth

Fig. 3 "Spiral crystal" having "milky way" pattern

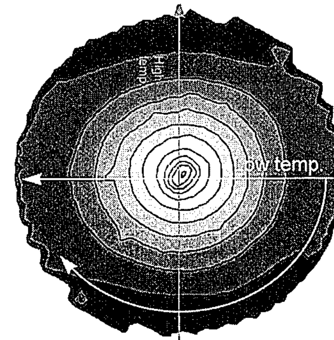

(a) Result of boundary shape measurement (in contours)

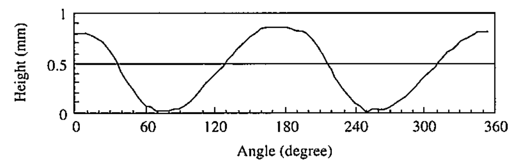

(b) Height fluctuation in circumferential direction

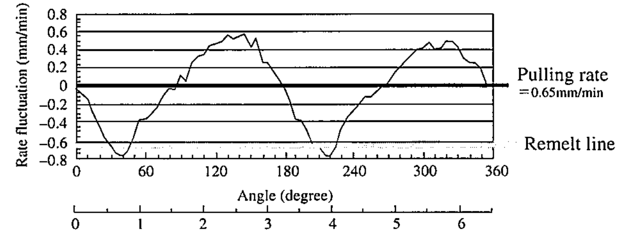

(c) Growth rate fluctuation in circumferential direction

Fig. 4 Result of 3-D measurement of solidification boundary

that remelting is occurring there.

6. Evaluation of "Spiral Crystals"

The "spiral crystals" were evaluated in two sections, namely, a vertical section parallel to the crystal growth direction and another section in right angles to the crystal growth direction (normal wafer slice section). Oxygen concentration was measured with a micro FTIR at intervals of 250 μm and, as for the resistivity (dopant concentration), spreading resistance was measured at intervals of 50 μm. Grown-in defects were examined by surface particle countering (COPs of 0.1 μm or larger), non-agitation Secco's etching (flow pattern defects - FPDs - and Secco etch-pit defects - SEPDs), infrared laser scattering tomography (laser scattering tomography defects - LSTDs) and infrared laser interferometer (optical precipitation profiler defects - OPP defects). Mitsui Mining's MO6 capable of identifying defects 0.08 μm in size down to a depth of 5 μm from the surface was used for the LSTDs. The OPP defects 0.08 μm or larger in size can be captured by focusing the device on a region 5 μm in diameter in the bulk.

Firstly, the distributions of resistivity, oxygen concentration and grown-in defects in the crystal growth direction were examined. Test pieces were prepared by vertically slicing a "spiral crystal" into 5 pieces at an interval of 20 mm in radial direction, and the test pieces were named Sample A to Sample E from the center to the edge. The distributions of the resistivity, oxygen concentration and OPP defects of the samples along the crystal growth direction are shown in **Figs. 5 and 6**. In Sample A taken from the center, the oxygen concentration fluctuated periodically, but the resistivity fluctuated only

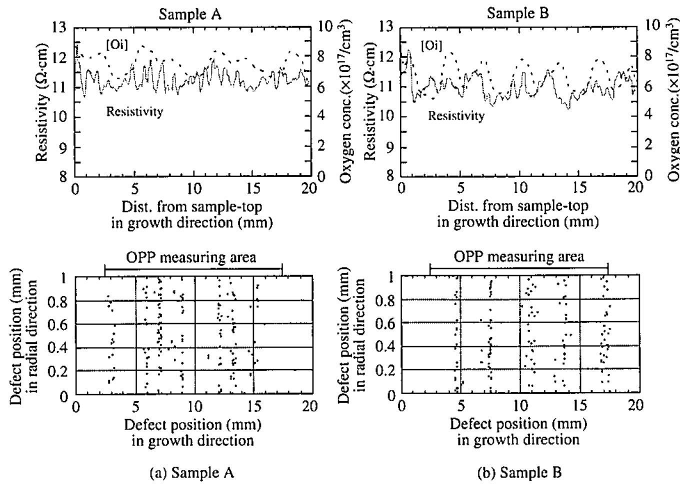

(a) Sample A (b) Sample B

Fig. 5 Distributions of oxygen concentration, resistivity and grown-in defects in crystal growth direction (1)

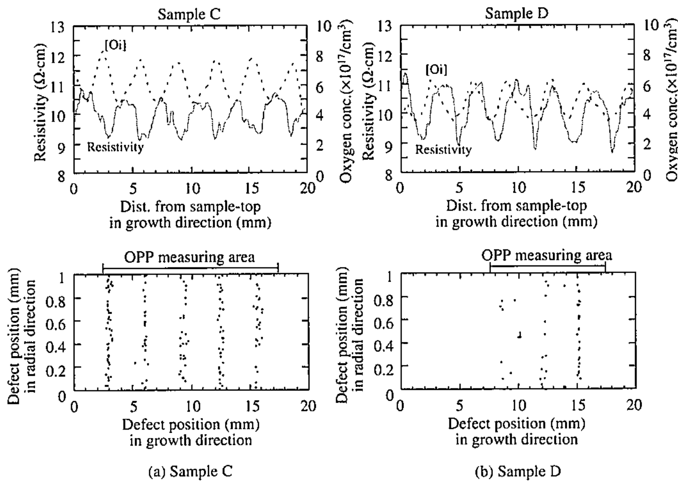

(a) Sample C (b) Sample D

(c) Sample E

Fig. 6 Distributions of oxygen concentration, resistivity and grown-in defects in crystal growth direction (2)

in a very narrow range, and no clear correlation was seen among the distributions of the resistivity, oxygen concentration and grown-in defects. In Samples B, C and D, the oxygen concentration and resistivity fluctuated periodically, and the nearer the edge the clearer the periodical fluctuations became, although the peaks of the oxygen concentration and resistivity did not always synchronize with each other but there were some lags between them.

The fluctuation period is roughly 6.5 mm, corresponding to a crystal growth in 10 min at a pulling rate of 0.65 mm/min, i.e., a growth in 1 crystal rotation. This indicates that the oxygen concentration and resistivity (dopant concentration) fluctuate due to the 2-fold symmetric temperature distribution at the melt surface. The grown-in defects in the samples are distributed, not in correlation with the oxygen concentration, but rather at the regions where the resistivity is low. Sample E, the nearest to the edge, showed the largest fluctuation amplitude of resistivity with a frequency similar to Samples B, C and D, while its oxygen concentration fluctuated within a small range. The grown-in defects of Sample E are distributed more at the regions where the resistivity is low but, since the defects are scattered more widely in the crystal growth direction, the correlation with the resistivity is not very clear. It is suspected that the wider distribution band of the grown-in defects was caused by rapid cooling at the crystal edge portion. In other words, defect nuclei could not grow in the edge portion due to rapid cooling, while their nucleation advanced even at low temperatures, thus the defects were distributed in wide ranges.

The difference in the behaviors of the resistivity and oxygen concentration is considered attributable to melt flow. The distribution of oxygen concentration is more affected by melt flow and SiO evaporation from the melt surface than by crystal growth rate and melt temperature. Vertical agitation does not occur easily inside an HMCZ crucible since only horizontal melt flows remain as a result of restriction of vertical flows. Oxygen in the melt evaporates at high temperatures forming SiO at the melt surface and, consequently, oxygen concentration of the melt falls there and thus the oxygen concentration of the portions of the crystal formed in these regions also falls. In this mechanism, oxygen is influenced more by the melt flow than temperature fluctuation. With regards to the dopant concentration, on the other hand, it is mainly determined by fluctuation of the melt temperature or crystal growth rate, since dopant evaporation from the melt is small. As a result, the concentration distributions of oxygen and dopant impurities do not completely synchronize with each other.

The above studies of the oxygen concentration, resistivity and defect distribution of the vertically sliced samples can be summarized as follows: oxygen concentration and resistivity fluctuate periodically at all the portions excepting the center but their respective frequencies have different phases; and the defects are distributed at the portions where the resistivity is low, or, the dopant concentration is high.

The crystal growth rate fluctuation based on the change in the resistivity was calculated using the BPS theory[31] and the following equation[32]:

$$\Delta C/C = (1 - k_0) * \Delta V * \delta / D$$

where δ is diffusion layer thickness expressed as $\delta = 1.6 * D^{1/3} * \omega^{-1/2} * \nu^{1/6}$, D is diffusion coefficient, ω is crystal rotation, ν is dynamic viscosity coefficient, ΔV is growth rate fluctuation, $\Delta C/C$ is dopant concentration fluctuation ratio, and k_0 is equilibrium segregation factor. The value of the growth rate fluctuation ΔV calculated from the resistivity fluctuation of Sample E is 0.68 mm/min, which is smaller than the value 1.25 mm/min of ΔV calculated from the boundary shape. We suspect that this is because the equation to calculate the diffusion layer thickness is not applicable when the crystal rotation is slow. Thus it was considered that the value of 1.25 mm/min (−0.8 to +0.45 mm/min) calculated directly from the crystal boundary shape

expresses the growth rate fluctuation more accurately.

Then, the grown-in defect distribution of the crystal non-agitation Secco's etching distributions of the FPDs and SEPDs were investigated. While the etching covered the entire wafer surface, the microscopic observation scanned, as shown with the arrow in **Fig. 7** (a), from the portion without COPs to the portion rich in COPs in a straight line. The scanning started from –65 mm and ended at +15 mm relative to the wafer centerline. The FPDs corresponded to the COPs, that is, the FPDs were found where COPs were densely distributed. In the other regions neither FPDs nor SEPDs were found and, besides, defects such as dislocations and small precipitates were also absent, meaning that perfectly defect-free regions were formed there.

Fig. 8 (a) is a defect distribution map of a "spiral crystal" drawn by the laser scattering tomography (LST). The detected grown-in defects are spread in wider areas than COPs, yet forming a kind of "milky way" pattern. Whereas the LST can detect the defects 0.08 μm or larger in size at depths up to 5 μm from the surface, a particle counter detects the defects 0.1 μm or larger in size on the wafer surface only. Therefore, the LSTD distribution is broader than COP distribution. An LST evaluation of defect size revealed that the defect size was small where defect concentration was high, and vice versa

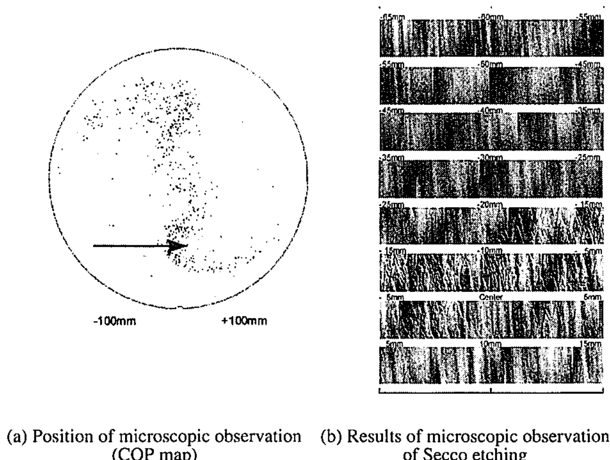

(a) Position of microscopic observation (COP map)
(b) Results of microscopic observation of Secco etching

Fig. 7 Results of Secco etching

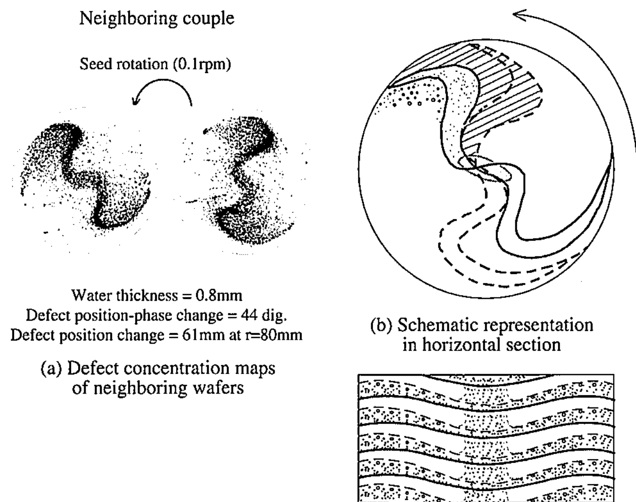

(a) Defect concentration maps of neighboring wafers

(b) Schematic representation in horizontal section

((c) Schematic representation in vertical section

Fig. 8 Grown-in defect distribution

where defect concentration was low. Sudden large fluctuations of defect concentration were seen at certain positions in a circumferential scanning of defect distribution, presumably due to drastic changes in the growth rate or melt temperature.

Fig. 8 (a) shows, side by side, the defect distributions of two wafers adjacent to each other in the longitudinal direction of a crystal. The distance between the two is 0.8 mm in the thickness direction, and the one in the right solidified earlier than the one in the left. The defect distribution in the crystal estimated from the observation results is schematically shown in a horizontal section (wafer surface) in Fig. 8 (b) and in a vertical section in Fig. 8 (c). The defect distribution changes spirally in the wafer thickness direction and defect-rich regions and defect-free regions appear alternately in a vertical section as seen in the schematic sectional view. Grown-in defects begin to form when the crystal solidification boundary passes through a low temperature region of the melt to form a high concentration zone of small defects.

After that, as the crystal grows and when the crystal solidification boundary passes through a high temperature region of the melt, defect formation is restricted and the defects tend to become large in size and low in concentration, finally resulting in a defect-free region. The "spiral crystal" is a result of these defect formation patterns repeated in the crystal growth direction. No peculiar defect distribution pattern is seen in the central regions presumably because there is no large change in the defect formation conditions there. The defect formation mechanism will be explained later in detail. Note that the defect distribution behavior described here is exactly identical to what was projected in the geometrical analysis in Section 4.

7. Summary of Test Results

The test results are summarized as follows:

(1) Grown-in defects well correspond with the resistivity fluctuation, i.e., the defects form in positions where the resistivity is low (dopant concentration is high). This is caused by the fluctuation of crystal growth rate due to the melt temperature distribution peculiar to the HMCZ. The position of low resistivity (high dopant concentration) is formed in the region where the crystal growth rate is high, whereas the position of high resistivity (low dopant concentration) is formed in the region where the crystal growth rate is low or where remelting occurs.

(2) The positions where the distributions of defects and dopant concentration suddenly change are formed when the crystal solidification boundary reaches a high temperature region of the melt.

(3) Oxygen concentration also changes periodically but its peaks are not in complete synchronization with those of resistivity.

8. Discussion of Defect Formation Mechanism

Fluctuation of dopant impurities is caused by the fluctuation of the crystal growth rate or the melt temperature. Dopant concentration is high in regions where the crystal growth rate is high, and vice versa where the crystal growth rate is low or remelting takes place. Grown-in defects form at the positions where the dopant concentration is high. Thus, it is suspected that the grown-in defects form in correlation with the fluctuation of growth rate or melt temperature. Here, The following three defect formation models in relation with these fluctuations were considered:

In a first model (called Model A), the Voronkov's parameter V/G (where V is growth rate and G is temperature gradient at the crystal solidification boundary) fluctuates. In a second model (called Model B), homogeneous nucleation rate and grown-in defect growth are

made to fluctuate by the melt temperature fluctuation. In a third model (called Model C), heterogeneous defect nucleation sites fluctuate, which sites are formed as a result of fluctuations of the melt temperature, growth rate, temperature gradient (G) and/or dopant concentration or as a result of interactions among these fluctuations.

Before studying these models, we carried out a simulation on how the melt temperature fluctuation affects V/G, the growth rate fluctuation, and fluctuation of the temperature gradient at the solidification boundary. The calculation is a simple non-steady finite differential crystal growth simulation, with application of the moving grid method, wherein the solidification boundary height, moving as a result of changes in the melt temperature condition, is shifted by re-defining the grids as proposed by Van Run et al. in their calculations[33]. As the boundary condition of a 1-dimensional coordinate, a temperature fluctuation of 1,437 ± 8°C was given to a fixed point of the melt at a period of 300 sec., and the Stefan condition was applied to the solidification boundary. The crystals were pulled at 0.65 mm/min, the same rate as the crystal growing tests. Based on the test data, the atmosphere temperature was set at 1,350 to 1,200°C. The calculation result is described below.

The crystal solidification boundary oscillates by about ± 3.5 mm due to the melt temperature fluctuation, and the crystal growth rate by ± 0.45 mm/min. While the melt temperature gradient fluctuates by ± 0.5°C/min, the crystal temperature gradient fluctuates by ± 0.025°C/min, which is only a very small fluctuation. The Voronkov parameter V/G is 0.13 ± 0.09 $mm^2/°C\cdot min$. Since G does not change widely, the value of V/G is determined mainly by the growth rate (V), and changes as V changes. Then, the concentration changes of dopant impurities and point defects were examined using Fick's diffusion equation and the above calculation result. Whereas boron and other dopants have comparatively low diffusivity in the order of 10^{-11} cm^2/s, point defects such as vacancies and interstitial atoms are fast diffusing species and they are reported to have diffusivity in the order of 10^{-4} to 10^{-6} cm^2/s.

Fig. 9 (a) shows the simulation result of dopant concentration. The concentration of boron to be absorbed in the crystal at the solidification boundary is made to fluctuate by the fluctuations of melt temperature and growth rate. Because boron has a low segregation coefficient, the concentration fluctuation near the solidification boundary is kept unchanged through crystal growth. Fig. 9 (b) shows the simulation result of the concentration of point defects such as vacancies and interstitial atoms. If a change in the absorption of point defects into the crystal takes place at the solidification boundary, the change is evened out due to the high diffusivity of point defects. As seen in Fig. 9 (b) where simulation results based on three different diffusivity values are shown, concentration fluctuation is evened out while the crystal grows by 100 mm from the solidification boundary even when the diffusivity D is as small as 10^{-6} cm^2/s.

The simulation results are summarized below. Melt temperature fluctuation causes fluctuations of crystal growth rate, the temperature gradient of the melt near the solidification boundary and V/G, the Voronkov parameter. (The temperature gradient of the crystal near the solidification boundary does not fluctuate much because of large thermal conductivity of the crystal.) Whereas unevenness of dopant concentration remains in the crystal, that of point defects is evened out during crystal growth within a short distance from the solidification boundary.

From the simulation results, Model A to explain defect distribution by the Voronkov parameter has to be discarded because it has been made clear that the point defect fluctuation disappears within

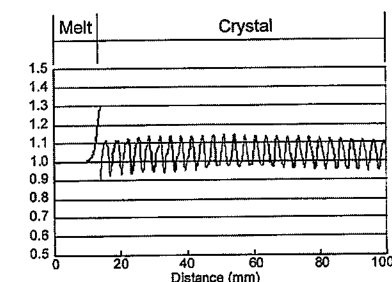

Distribution of dopant concentration in growth axial directic

(a) Simulation result of dopant concentration ($D = 10^{-11}$ cm^2/s)

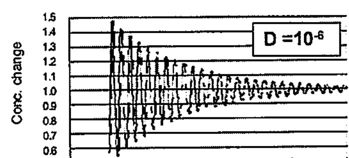

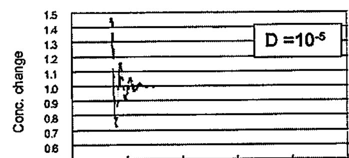

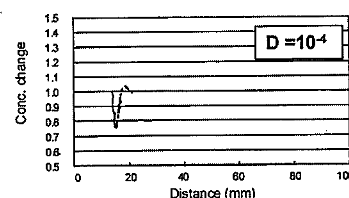

(b) Simulation result of point defect concentration fluctuation (Calculated for point defect diffusivity values of 10^{-4}, 10^{-5} and 10^{-6} cm^2/s based on past reports.)

Fig. 9 Change of impurity concentration in crystal

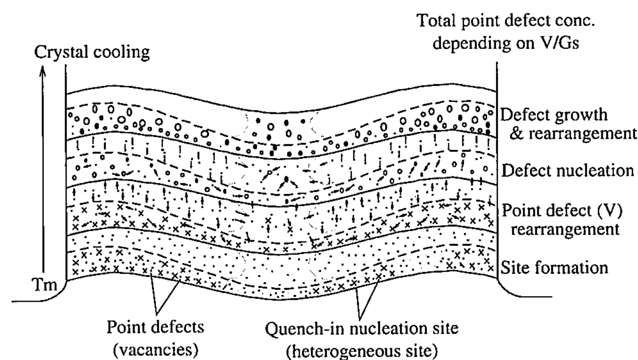

Fig. 10 Schematic representation of defect formation mechanism model

100 mm of crystal growth due to large diffusivity of the point defects, although the value of V/G changes following change of the growth rate (V). It has been known that the nucleation and growth of grown-in defects, or void defects, occur in a narrow temperature range from 1,150 to 1,050°C. But, the temperature range this report deals with where the defect distribution is formed is near the solidification boundary and, hence, it is higher than the above. The effect of the temperature fluctuation at the solidification boundary does not extend to the temperature range related to the nucleation and growth of grown-in defects. Consequently, Model B supposing fluctuations of the nucleation and growth of defects caused by fluctuation of melt

temperature is also inappropriate. **Fig. 10** schematically shows Model C we propose as the most suitable one, wherein heterogeneous void nucleation sites are formed near the solidification boundary.

The sites are formed when the solidification boundary passes through a low temperature region of the melt temperature distribution, but they disappear due to rapid overheating or remelting of the solidification boundary when it enters a high temperature region from a low temperature region. Lattice imperfection is caused by fluctuation of the melt temperature, growth rate or dopant concentration, and this lattice imperfection is suspected be a factor to from the sites. The lattice imperfection (void nucleation sites) increases in regions where the crystal growth rate is raised. Point defects (vacancies) diffuse during crystal cooling at comparatively high temperatures, and they are trapped in the void nucleation sites and re-arranged along the sites. In this manner, defects become densely concentrated in regions having the void nucleation sites, and defect-free portions are created in regions having no void nucleation sites. The "milky way" pattern and the "double spiral" pattern are formed by the unique band (grown-in defect nucleation sites) at the solidification boundary.

Although the Voronkov parameter well explains macroscopic behavior of point defects in the normal CZ process without application of the magnetic field, it is necessary to take into consideration also the presence of the heterogeneous defect nucleation sites this report proposes. Our future task is to identify the heterogeneous defect nucleation sites, namely, the lattice imperfection formed at the solidification boundary.

9. Conclusion

Microscopic defects can be intentionally distributed in a "milky way" pattern or a "double spiral" pattern by growing crystals in the CZ process with a horizontal magnetic field (HMCZ) at a very slow rotation rate. The wafers thus manufactured have grown-in defect-rich regions and defect-free regions. The defect distribution is formed in the low temperature band at the solidification boundary peculiar to the HMCZ.

that the Heterogeneous defect nucleation sites are suspected to be formed at the solidification boundary when it passes through low temperature regions of the melt. In fact, formation of the grown-in defects corresponds with fluctuation of resistivity and is not correlated with oxygen concentration. The fluctuation of resistivity is caused by fluctuation of growth rate, and so is the defect formation. The fluctuation of growth rate is affected directly by melt temperature fluctuation at the crystal solidification boundary. It so follows that the formation of the heterogeneous defect nucleation sites at the solidification boundary is caused by the fluctuation of growth rate, and the sites increase when the crystal grows rapidly, that is, when the solidification boundary passes through a low temperature zone of the melt, and the sites decrease and finally disappear when the crystal grows slowly or it remelts, that is, when the solidification boundary passes through a high temperature zone of the melt. Control of the heterogeneous defect nucleation sites this paper proposes is an important factor in the control of grown-in defects, besides the Voronkov's parameter V/G widely used presently for the purpose.

References

1) Abe, T. et al. : Jpn. J. Appl. Phys. 5, 458 (1966)
2) de Kock, A. J. R. et al. : J. Cryst. Growth. 22, 311 (1974)
3) de Kock, A. J. R. et al. : J. Cryst. Growth. 30, 279 (1975)
4) Abe, T. et al. : Physica. 116B, 139 (1983)
5) Harada, H. et al. : Semiconductor Silicon. 1986, p.76
6) Ryuta, J. et al.: Jpn. J. Appl. Phys. 29, L1947 (1990)
7) Hasebe, M. et al.: Proc. Int. Conf. Defect Control in Semiconductors. 1989, p.157
8) Yamauchi, T. et al.: Jpn. J. Appl. Phys. 31, L439 (1992)
9) Shinoyama, S. et al.: OYOBUTURI. 60, 766 (1991)
10) Petroff, P. M. et al. : J. Cryst. Growth. 36, 4 (1976)
11) Voronkov, V. V. : J. Cryst. Growth. 59, 625 (1982)
12) Habu, R. et al. : Jpn. J. Appl. Phys. 32, 1740 (1993)
13) de Kock, A. J. R. : Philips Res. Rept. Suppl. 1, 1 (1974)
14) Chikawa, J. et al. : Jpn. Appl. Phys. 18, Suppl. 18-1, p.163 (1979)
15) Roksnoer, P. J. et al.: J. Cryst. Growth. 53, 563 (1981)
16) Osaka, J. et al.: Appl. Phys. Lett. 36, 288 (1980)
17) Inoue, N. et al.: J. Electrochem. Soc. 129, 2780 (1982)
18) Kishuno, S. et al.: J. Appl. Phys. 21, 1 (1982)
19) Abe, T. et al.: J. Jpn. Accoc. Cryst. Growth. 13, 122 (1986)
20) Park, J-G. et al.: Semiconductor Silicon. 1994, p.370
21) Itsumi, M. et al.: J. Appl Phys. 78, 5984 (1995)
22) Kato, M. et al.: Jpn. J. Appl. Phys. 35, 5597 (1996)
23) Yamagishi, H. et al.. : Proc. Symp. on Adv. Sci. and Tech. of Silicon Materials, p.83
24) Umeno et al.: Jpn. J. Appl. Phys. 32, L699 (1993)
25) Nakajima et al.: Semiconductor Silicon. 1994, p.168
26) Takano, K. et al.: Abstracts of Fall Mtg. Jpn. Soc. Appl. Phys. 19p-ME-4, 1994
27) Kimura, M. et al.: Abstracts of Fall Mtg. Jpn. Soc. Appl. Phys.2p-N-8, 1997
28) Ishikawa, F. et al.: Abstracts of Fall Mtg. Jpn. Soc. Appl. Phys.2p-N-9, 1997
29) Iino, E. et al.: Abstracts of Fall Mtg. Jpn. Soc. Appl. Phys.27-ST-27, 1995
30) Ishikawa, F. et al.: Abstracts of Spring Mtg. Jpn. Soc. Appl. Phys. 30a-YA-3, 1998
31) Burton, J. A. et al.: J. Chem. Phys. 21, 1987 (1953)
32) Murgai, A. et al.: J. Electrochem. Soc. 126, 2240 (1979)
33) Van Run, A. M. J. G. : J. Cryst. Growth. 54, 195 (1981)